

pubs.acs.org/JPCB Article

Understanding the Hydration Thermodynamics of Cationic Quaternary Ammonium and Charge-Neutral Amine Surfactants

Published as part of The Journal of Physical Chemistry virtual special issue "Pablo G. Debenedetti Festschrift". Himanshu Singh and Sumit Sharma*



Cite This: https://doi.org/10.1021/acs.jpcb.2c03562



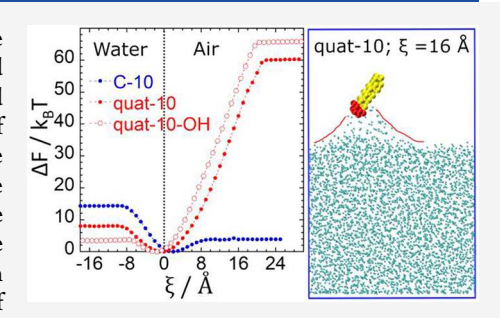
ACCESS I

III Metrics & More

Article Recommendations

SI Supporting Information

ABSTRACT: Aqueous solubility and interfacial adsorption of surfactants are important for numerous applications. Using molecular dynamics, we have studied the effect of the type of the polar headgroup (cationic quaternary ammonium and charge-neutral amine) and length of the alkyl tail on the hydration free energy of surfactants in infinite dilution. In addition, we have studied the effect of replacing the terminal methyl group of the alkyl tail with a more polar hydroxyl group on the hydration free energy. Quaternary ammonium surfactants have strongly favorable hydration free energies, whereas charge-neutral amine surfactants have unfavorable hydration free energies. The contribution of the quaternary ammonium group in reducing the hydration free energy is estimated to be as large as $\sim 63~k_BT$ and that of the charge-neutral amine group to be 3 k_BT . Both surfactants and their corresponding



alkanes have minima in the free energy at the air—water interface. The quaternary ammonium group contributes to a $6\ k_BT$ decrease in the free energy of transfer from air—water interface to bulk aqueous phase (termed henceforth as interface transfer free energy). The amine group, on the other hand, has a net zero interface transfer free energy. The interface transfer free energies of surfactants are both enthalpically and entropically unfavorable. The enthalpic penalty is attributed to the loss of water—water interactions. Interestingly, surfactant molecules gain entropy upon their transfer from the air—water interface to the aqueous phase, but this increase is more than compensated by the loss in the entropy of water molecules, presumably due to the ordering of water molecules around the surfactants. Replacing the terminal methyl group of the alkyl tail with a hydroxyl group in quat surfactants reduces their hydration free energy by $10\ k_BT$, thus making them more soluble in water. Attaching a hydroxyl group to the alkyl tail also inhibits their micelle forming tendency in the bulk aqueous phase. Overall, this work reveals how tuning the molecular characteristics of surfactants can help to achieve the desirable aqueous solubility, interfacial properties, and micellization tendency of surfactants.

1. INTRODUCTION

Surfactants, or surface-active agents, are amphiphilic molecules with a polar headgroup and a hydrocarbon tail. The polar headgroup prefers to be solvated in water, whereas the hydrocarbon tail is hydrophobic. Surfactants are used in innumerable applications including detergency, froth floatation,² synthesis of anisotropic metal nanoparticles,³ corrosion inhibition, enhanced oil recovery, and lubrication. For these applications, it is desirable that surfactant molecules have appreciable aqueous solubility so that they are available in the aqueous phase to adsorb onto solid-water or oil dropletwater interfaces. Poorly soluble surfactants phase separate out of the aqueous medium,^{7,8} or get trapped at unwanted interfaces without being able to reach to the interfaces where they are intended to adsorb. For instance, surfactant molecules are added to oil-and-gas pipelines to reduce internal corrosion of the pipelines from the trace amount of water present in the oil/gas stream. These molecules mitigate corrosion by adsorbing onto the metal surface and forming a barrier to the ingression of water molecules. For efficient corrosion inhibition, surfactant molecules that are added to the pipelines should have sufficient aqueous solubility to adsorb on to the metal—water interface rather than aggregating at the oil/gas—water interfaces, which would render them ineffective. ^{9–17} Therefore, improving the aqueous solubility of surfactants is a worthwhile pursuit for many applications.

Numerous factors influence the aqueous solubility of surfactants. Increased salinity and low pH have been shown to enhance aqueous solubility of cationic surfactants. ^{13,15,17} Ionic surfactants have higher aqueous solubility as compared to nonionic surfactants of the same alkyl tail because of the strong tendency of ionic head groups to be solvated in water. ^{18,19} Studies have reported hydration free energies of surfactants and alkanes to linearly increase with the addition of each

Received: May 23, 2022 Revised: October 31, 2022



methylene group 19-26 and decrease with the size of the polar headgroup. 24

Nonionic surfactants, though less water-soluble, may be preferred in some applications, such as corrosion inhibition, because of their tendency to adsorb at the metal-water interfaces in high-density adsorbed morphologies. For example, charge-neutral decanethiol molecules adsorb at metal-water interfaces much better than cationic alkyl dimethyl benzyl ammonium bromide molecules, but they have lower aqueous solubility.^{27,28} Hydrophobic interactions between the alkyl tails are deemed important for the free energy of aggregation of surfactant molecules at the air/oil-water interfaces. 19 Computational and experimental works reveal that hydrophobic interactions between long alkyl tails of surfactant molecules facilitate formation of high-density adsorbed morphologies at metal-water interfaces.^{29,30} Long alkyl tail surfactants also have a tendency to aggregate as micelles above their critical micelle concentration, and in this form, they may not adsorb at metal-water interfaces. We have previously reported that cationic surfactant micelles experience a longrange free energy barrier to adsorption at metal—water interfaces.^{31,32} Thus, the adsorption characteristics at the metal-water interface, aqueous solubility, and micellization tendency of surfactants often evolve orthogonally in molecular design.

In most applications, including corrosion inhibition, enhanced oil recovery and synthesis of anisotropic metallic nanoparticles, surfactants are added in parts-per-million (ppm) level concentrations. To model the partitioning of surfactants in the aqueous phase at these concentrations, the hydration free energy calculated at infinite dilution is an excellent approximation. In this work, we have performed molecular dynamics (MD) simulations to study the effect of the type of the polar headgroup (cationic quaternary ammonium and charge-neutral amine) and length of the alkyl tail of surfactants on their hydration free energy and the free energy of transfer from air-water interface to bulk aqueous phase (termed as interface transfer free energy) in infinite dilution. In addition, we have studied the effect of replacing the terminal methyl group of the alkyl tail with a more polar hydroxyl group on these free energies. We show that quaternary ammonium surfactants have highly favorable hydration free energies, whereas alkanes and charge-neutral amine surfactants have unfavorable hydration free energies. Both the surfactants and alkanes have lowest free energy at the air-water interface. The cationic quaternary ammonium group contributes to a decrease in the hydration free energy by $\sim 63 k_B T$ and a decrease in the interface transfer free energy by 6 k_BT . Interestingly, the charge-neutral amino group has zero net interface transfer free energy but it contributes to reducing the hydration free energy by 3 k_BT . Furthermore, we show that replacing the terminal methyl group of the alkyl tail with a hydroxyl group significantly increases the aqueous solubility of the surfactants. Addition of a hydroxyl group to the alkyl tail also decreases the micellization tendency of the surfactant molecules. These results demonstrate that the solubility and aggregation characteristics of long alkyl tail surfactants can be tuned by simple point substitutions.

2. SIMULATION SYSTEM AND METHODS

Parts a-d of Figure 1 show the surfactant and the alkane molecules that we have studied using MD simulations. The molecules are cationic quaternary ammonium-based surfac-

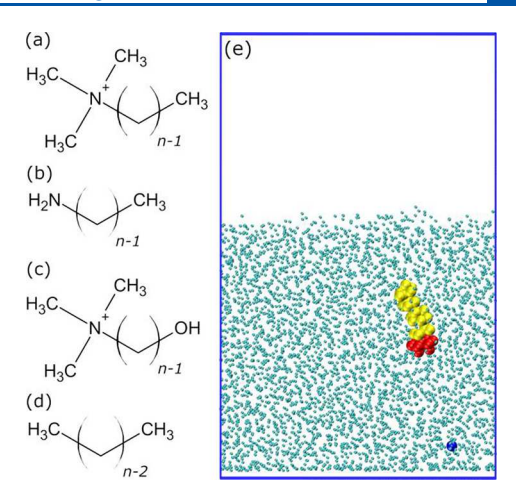


Figure 1. Structure of the (a) quat-n molecules (n = 10/16 for quat-10/qquat-16), (b) amine-n molecule (n = 10 for amine-10), (c) quat-nOH molecules (n = 10/16 for quat-10OH/quat-16OH), and (d) C-n molecules (n = 10/16 for C-10/C-16). (e) Snapshot of the simulation system with a quat-10 molecule in the aqueous medium. The red beads represent the polar headgroup of the molecule, the yellow beads represent the hydrophobic alkyl tail, the blue bead represents the chloride counterion, and the small cyan dots represent water oxygens.

tants (henceforth referred to as quat-n) [Figure 1a], an uncharged amine-based surfactant (henceforth referred to as amine-n) [Figure 1b], cationic quaternary ammonium-based surfactant molecules with a terminal hydroxyl group (henceforth referred to as quat-n-OH) [Figure 1c], and linear alkane molecules (henceforth referred to as C-n) [Figure 1d], where n denotes the length of the tail of the molecules. The quat and amine molecules are chosen because they are widely used in the synthesis of anisotropic nanoparticles and for corrosion inhibition in oil and gas pipelines. 33-35 The MD simulations are performed in a two-phase system comprising of liquid water and its vapor phase. A snapshot of the simulation system with a quat-10 molecule in the liquid phase is shown in Figure 1e. We do not have any N2 and O2 molecules in the vapor space, but water molecules are free to enter this space. Since water vapor density is 1000 times smaller than the liquid density, therefore 1 to 2 water molecules intermittently enter this space.

The simulation box is periodic in the x- and y- directions, but nonperiodic in the z- direction, and has dimensions of $52.61 \text{ Å} \times 52.61 \text{ Å} \times 100 \text{ Å}$. The nonperiodicity is maintained by placing two walls at z = 0 and z = L, where L is the length of the simulation box in the *z*- direction. The wall at z = 0 has an attractive interaction with the water molecules so that the water column remains pinned to the z = 0 surface. In the absence of the attractive surface at z = 0, the water column may get laterally displaced in the z-direction because of the interactions between water and the surfactant molecule. The attractive interaction potential is in the form of a 9-3 function, which is essentially an integrated Lennard-Jones potential [eq S1, Supporting Information]. The bottom wall is reflective and nonattractive to all other species of the system. The wall at z =L is athermal/reflective to all the atoms in the system. The interaction potential parameters of the surfactant and the alkane molecules are obtained from the General Amber force field (GAFF).³⁶ Other accurate force fields also exist for alkanes, such as the TraPPE-United Atom (UA). We show in

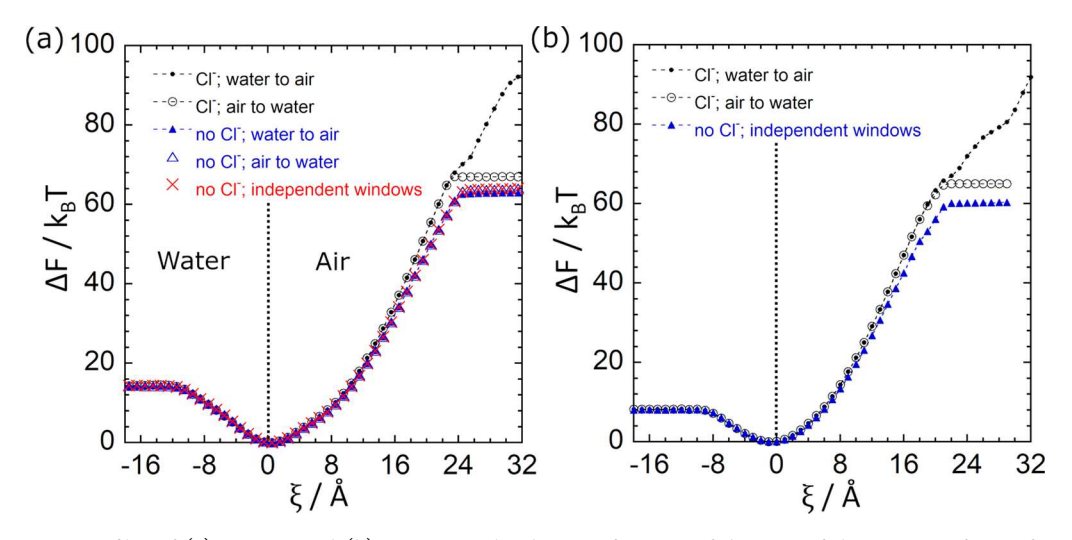


Figure 2. Free energy profiles of (a) quat-16 and (b) quat-10 molecules as a function of distance of their center-of-mass from the air—water interface. The air—water interface is at $\xi = 0$ Å, and is marked by a vertical dotted line. The black colored profiles belong to the charge-neutral system in which a chloride ion is present, and the blue/red profiles belong to the charged system in which the chloride is absent. In the charge-neutral system, hysteresis in the free energy profiles is observed beyond $\xi \approx 23$ Å. In the absence of chloride, that is the charged system, the profiles obtained from both the umbrella sampling paths overlap with each other and also with the profile in which the initial configurations for the umbrella sampling windows are generated independently ("independent windows", see text for more details). Error estimates of the profiles are within 0.3 $k_B T$ and are not shown for the sake of clarity of the overlapping profiles.

section 3.5 that the hydration free energies of alkanes remain invariant between the choice of GAFF and TraPPE-UA force fields. Partial charges on the surfactant atoms are computed from density functional theory (DFT) by employing B3LYP hybrid functional with 6-31G(d,p) basis set. The DFT calculation is performed in implicit water using Gaussian 16.37 In Gaussian 16, a self-consistent reaction field is used to account for the effect of a polarizable solvent. For water, a dielectric constant of $\varepsilon = 78.3553$ is used. The partial charges and the interaction potential parameters of the atoms of the studied surfactants and alkanes are provided in Figures S1 and S2 [Supporting Information]. In the MD simulations, explicit water molecules are employed which are represented via the extended simple point charge model (SPC/E).³⁸ Since quat molecules are cationic, their simulation system has a net +1e charge in the absence of a counterion. The hydration behavior of quat molecules is studied in both charged as well as chargeneutral systems. In the charged system, a compensating background charge is intrinsically applied by the MD package thereby maintaining the system at finite energy. To study the charge-neutral system of quat molecules, a chloride ion is introduced as a counterion. The potential parameters of the chloride ion are taken from the Joung-Cheatham model.³⁵ Simulations are performed in the isothermal-isochoric ensemble at T = 300 K, wherein the number of atoms (N), volume (V), and temperature (T) of the system are held fixed. The presence of a vapor space adjacent to the water column ensures that the system pressure is maintained at the saturation pressure corresponding to the fixed temperature. 40 For simplicity, the vapor phase is henceforth referred to as the air phase. Surfactant and alkane molecules experience Brownian dynamics in air. 41 Therefore, their motion in air is simulated using Langevin dynamics. The damping coefficient for Langevin dynamics is taken as 0.00125/ps for each surfactant/alkane atom, based on the prior experimental and simulation works. 42,43 The cutoff distance for Lennard-Jones and short-range part of Coulombic potentials is taken as 10 Å. The long-range part of Coulombic potential is computed using the particle–particle particle-mesh (pppm) Ewald summation method. The number of water molecules in the system is 4,382. The surfactant and the alkane molecules are simulated in infinite dilution. All simulations are performed using the large-scale atomic/molecular massively parallel simulator (LAMMPS).⁴⁴

Free energy profiles of the molecules across the air—water interface are generated using umbrella sampling. Air—water interface is defined as the location where the average density of water molecules is 0.5 g/cm³ [Figure S3, Supporting Information]. This location is marked as $\xi = 0$ Å. In the umbrella sampling technique, a harmonic biased potential is applied to the center-of-mass of the molecules, given by

$$U(\xi, \, \xi_0) = \frac{1}{2}k(\xi - \xi_0)^2 \tag{1}$$

where k is the force constant, ξ_0 is the set position of the center-of-mass of molecule from the air–water interface, and ξ is the instantaneous position of the molecule in a configuration. The biased potential is applied using the Colvars implementation in LAMMPS. 46 We choose $k = 5 \text{ kcal/mol/Å}^2$, and generate umbrella sampling windows by changing ξ_0 in the increments of 0.5 Å. We find that this interval is sufficiently small that overlapping histograms of the sampling distributions are obtained [Figure S4, Supporting Information]. Weighted histogram analysis method (WHAM) is then invoked, which combines all the biased simulations and produces the free energy profile based on the unbiased probabilities.⁴⁷ All the umbrella sampling simulations are first run for 20 ns to let the system reach equilibrium, and then run for another 20 ns for the calculation of thermodynamic properties. Three independent simulations are performed at each umbrella sampling window and correspondingly three independent free energy profiles are generated. The three independent free energy profiles are found to overlap with each other, confirming that the free energy profiles are converged. The estimated errors in the free energy profiles are found to be less than 0.3 k_BT . To check for hysteresis, for the quat-16 molecule, two estimates of

the free energy profile are generated for both the charged and the charge-neutral systems. The first, termed as "water-to-air", is generated using the set of initial configurations obtained from a steered MD simulation where the quat molecule is moved from water to air at the velocity of 0.5 Å/ns. The "air-to-water" estimate of the free energy profile is analogously defined. In addition, we also generated the free energy profile without following any steered MD path for initial configurations but by placing the quat molecule initially at different random locations in the simulation box for different umbrella sampling windows. Thus, the initial configurations in this case are independent of each other. This estimate of the free energy profile is termed as "independent windows".

3. RESULTS AND DISCUSSION

3.1. Free Energy Profiles of Quaternary Ammonium and Amine Surfactants across the Air—Water Interface.

Free energy profiles of the cationic quat (quat-16 and quat-10) molecules as a function of distance of their center-of-mass from the air—water interface, ξ are shown in Figure 2a and Figure 2b, respectively. The profiles are obtained for both the charged (with no Cl⁻) as well as the charge-neutral (with Cl⁻) systems. For the charged quat-16 system, the "water-to-air", "air-to-water", and "independent windows" estimates of the free energy profile overlap [Figure 2a]. Therefore, for the charged system, it suffices to consider the "independent windows" estimate of the free energy profiles. For the charge-neutral systems, the "water-to-air" and "air-to-water" estimates match up until $\xi \approx 23$ Å and then deviate for $\xi > 23$ Å. The reason for the hysteresis observed for the charge-neutral systems is explained after a discussion of the main features of these free energy profiles.

The free energy for both quat molecules is minimum at the interface, implying that the interface is their preferred location. The free energy profiles of the molecules rise rapidly in the air as a convex function, i.e., $\Delta F''(\xi) > 0 \ \forall \ \xi > 0$ Å. The reason is that when the quat molecules are in the air but close to the interface, their polar head groups point toward the interface and remain solvated with the water molecules. As a result, there is development of a nanoscopic water finger at the air—water interface, which increases the interfacial area of the air—water interface [Figure 3]. This increase in the air—water interfacial area results in large increase in the free energies beyond $\xi = 0$ Å.

Parts a and b of Figure 2 show that in the presence of chlorides (that is, for the charge-neutral system), the "water-to-air" estimate of the free energy profile differs from the "air-to-

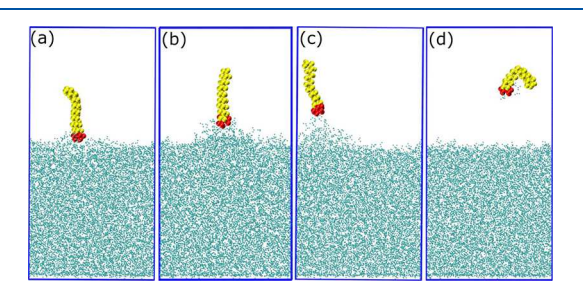


Figure 3. Snapshots of the charged system with quat-16 at (a) $\xi = 12.5$ Å, (b) $\xi = 16$ Å, (c) $\xi = 24$ Å, and (d) $\xi = 26$ Å. A water finger is observed starting from $\xi \approx 12.5$ Å, which grows up to $\xi \approx 24$ Å and then breaks. In part d, a few water molecules can be seen in the air near the charged headgroup.

water" estimate beyond $\xi \approx 23$ Å. This suggests that the choice of umbrella sampling path gives rise to a hysteresis in the free energy profiles. Figure S5 [Supporting Information] shows snapshots of the simulation system in the region $\xi \gtrsim 23$ Å. For the "air-to-water" estimate, the quat-16 molecule in bulk air has the counterion bound to the polar headgroup via Coulombic interactions [Figure S5a, Supporting Information]. The free energy remains constant until $\xi \approx 23$ Å, when the counterion goes into water and a water finger is formed. It is observed that the water finger does not form when the counterion stays with the quat molecule. Once the water finger is formed, the free energy decreases gradually as the quat molecule is moved toward the interface. For the "water-to-air" estimate, in our simulation time frame (\sim 40 ns), the counterion stays in water even when the quat molecule is moved beyond $\xi \approx 23$ Å. Interestingly, the water finger keeps growing beyond $\xi \approx 23$ Å.

To avoid the problem of hysteresis in the free energy profiles, we have focused on analyzing only the charged system for the hydration of quat molecules [Figure 2a,b]. In the charged system [Figure 3], the water finger breaks at around $\xi \approx 24$ Å and the free energy profile becomes flat beyond $\xi \gtrsim 24$ Å. The snapshots in Figure 3 confirm that the increase in the free energy beyond $\xi \gtrsim 12$ Å is because of the growth of the water finger. It is worth noting that the free energy does not drop when the water finger breaks at $\xi \approx 24$ Å, but remains flat

Free energy profiles of the quat molecules, along with the uncharged amine (amine-10) and alkane (C-10 and C-16) molecules are shown in Figure 4a. We acknowledge that the hydration free energies calculated in the simulations for alkanes deviate from the experimental values, 21,25 but we get the correct trends. The free energy profiles of amine-10 and alkane molecules are not long-ranged convex functions beyond $\xi > 0$ Å as is the case with the quat molecules. It is because the amine-10 and alkane molecules are uncharged, and therefore do not pull a water finger toward themselves [Figure S6b,c, Supporting Information]. There is an increase in the free energy of amine and alkane molecules beyond $\xi > 0$ Å, which is attributed to the loss of favorable Lennard-Jones interactions between the surfactant/alkane and water molecules. The free energy change to the transfer from the bulk air to water is referred as the hydration free energy (denoted as ΔF_{hyd}), and the free energy to transfer from the air-water interface to bulk water is referred as the interface transfer free energy (denoted as $\Delta F_{i/w}$), where the subscript i/w represents interface/water. Figure 4b shows ΔF_{hyd} and $\Delta F_{i/w}$ of the molecules. Since alkanes are hydrophobic, they have an unfavorable ΔF_{hvd} . The quat molecules, on the other hand, have a highly favorable ΔF_{hvd} . This matches with the experimental results, which reported that, in a two phase water-oil system, quat molecules stay in the water phase and do not enter the oil phase.14 Change in the $\Delta F_{i/w}$ of both the quat molecules is smaller by 6 k_BT in comparison to their corresponding alkanes. The larger $\Delta F_{i/w}$ of quat-16 is due to its longer alkyl tail.

The $\Delta F_{i/w}$ of the amine-10 and C-10 molecules are the same. The amine headgroup, therefore, does not contribute to the free energy of transfer from the interface to water. It is interesting to note that the ΔF_{hyd} of the amine-10 molecule is lower than that of the C-10 molecule. The amine molecule has larger preference to be at the interface as compared to C-10 as the amine group gets solvated at the interface. The ΔF_{hyd} of both amine-10 and C-10 molecules are unfavorable and are 7.5 k_BT and 10.4 k_BT respectively. This aligns with the

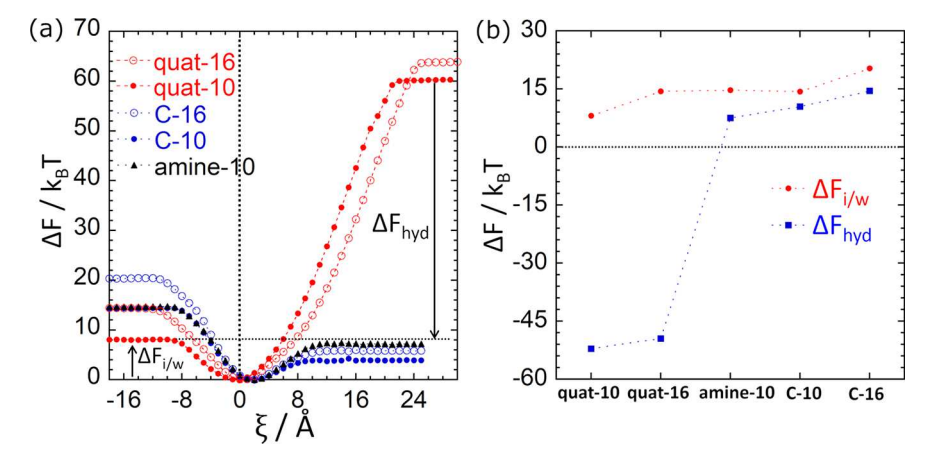


Figure 4. (a) Free energy profiles of quat-10, quat-16, amine-10, C-10, and C-16 molecules as a function of the distance of their center-of-mass from the air—water interface, ξ . The air—water interface is at $\xi = 0$ Å, and is marked by a vertical dotted line. Quat molecules show good aqueous solubility and poor affinity for air, whereas the amine molecule prefers to be in air than water. The free energy profiles of quat molecules have a long-ranged convexity in the air, i.e., $\Delta F''(\xi) > 0 \, \forall \, \xi > 0$ Å, whereas the amine molecule does not show such a long-ranged convexity. The interface transfer free energy, $\Delta F_{i/w}$ of the quat-10 molecule (that is, the change in the free energy to go from its free energy minimum location, $\xi = -1$ Å, to bulk water) and the hydration free energy, ΔF_{hyd} (that is, the change in the free energy to go from the air to bulk water) are shown by the two arrows. (b) Comparison of the $\Delta F_{i/w}$ and ΔF_{hyd} values of the studied molecules in part a. The size of the error bars in the free energy values in parts a and b are within 0.3 $k_B T$ and are therefore smaller than the size of the markers. The ΔF_{hyd} values for alkanes obtained in our simulations deviate from the experimentally known values. However, in the estimate of the effect of the polar group on the change in ΔF_{hyd} , the contribution of the alkyl tail cancels out.

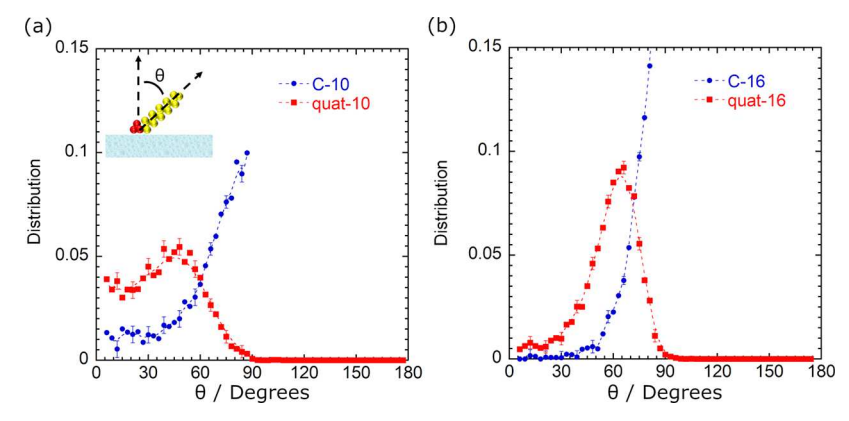


Figure 5. Distribution of the orientation of (a) quat-10 and C-10 and (b) quat-16 and C-16 molecules at the air—water interface. For the quat molecules, θ is the angle between the interface normal and the vector joining the nitrogen of the polar headgroup to the carbon of the terminal methyl group (shown in the inset image). For alkanes, θ is the angle between the interface normal and the vector joining the terminal carbon atoms. Since the terminal groups of the alkanes are the same, the configuration of the alkanes at θ is indistinguishable from their configuration at $180^{\circ} - \theta$. Therefore, orientation distribution of the alkanes is shown for the range $0^{\circ} \le \theta \le 90^{\circ}$. The profiles are normalized by $\sin(\theta)$. The peaks in the profiles suggest that the alkanes lie parallel to the interface ($\theta = 90^{\circ}$), whereas the quat molecules are tilted with their hydrophobic tails protruding away from the interface ($\theta \lesssim 60^{\circ}$ for quat-10 and $45^{\circ} \lesssim \theta \lesssim 75^{\circ}$ for quat-16). The orientation distribution of quat molecules in bulk water is shown in Figure S9 [Supporting Information].

experimental observations that uncharged surfactant molecules with long alkyl tails have higher solubility in the oil phase as compared to the aqueous phase. The hydration behavior of uncharged surfactant molecules contrasts with those of the charged quat molecules as charged quat molecules show a strongly favorable free energy to enter the aqueous phase from the air.

The free energies of quat-10, quat-16, amine-10 and C-10 molecules are minimum at $\xi = -1$ Å, 0 Å, 2 and 2 Å respectively. At these locations, the quat and amine molecules are oriented such that their polar head groups are submerged in water, and their hydrophobic tails protrude toward air. The C-10 molecule, on the other hand, lies on the air-side and is parallel to the interface. This is demonstrated by the distribution profiles of orientation of the quat and alkane

molecules at their respective free energy minima locations as shown in Figure 5, parts a and b. The orientation of the molecules is shown by θ , where θ is the angle that the molecules make with the interface normal. The spatial distributions of the quat and amine molecules at their free energy minima locations are shown in Figures S7a,b and S8a [Supporting Information].

3.2. Enthalpy and Entropy of Hydration of Quaternary Ammonium and Amine Surfactants. The enthalpy profiles are computed using the relation

$$\Delta H = \Delta U + \Delta (PV) \tag{2}$$

where ΔU is the total internal energy of the system. At constant pressure, $V\Delta P=0$. Also, since $P\Delta V\approx 0$, $\Delta H\approx \Delta U$. Figure 6a shows the ΔU profiles of the quat, amine surfactants

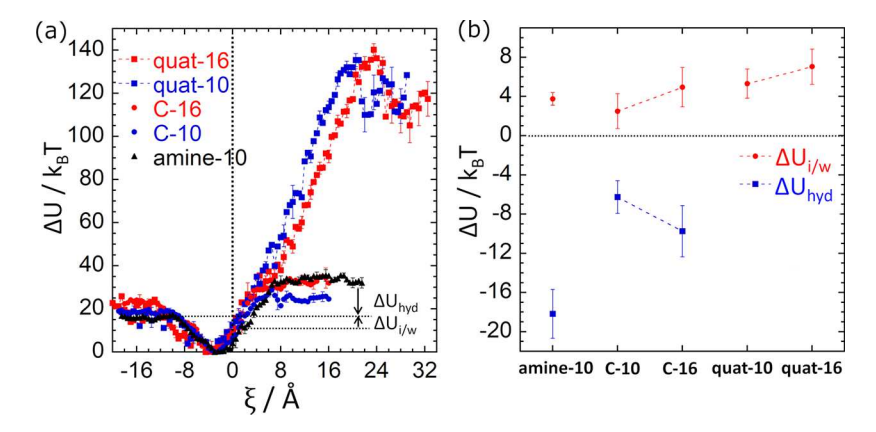


Figure 6. (a) Enthalpy profiles of the quat, amine, and alkane molecules as a function of the distance of their center-of-mass from the air—water interface, ξ . The transfer enthalpy of the amine-10 molecule (that is, the change in the enthalpy to go from its free energy minimum location, $\xi=2$ Å to bulk water) is shown by an arrow. Also shown is the hydration enthalpy, ΔU_{hyd} of the amine-10 molecule. (b) Comparison of the $\Delta U_{i/w}$ and ΔU_{hyd} values of the studied molecules in part a. Because of the large fluctuations in the enthalpy profiles of quat molecules beyond $\xi \gtrsim 23$ Å, the ΔU_{hyd} values of the quat molecules are not shown in part b.

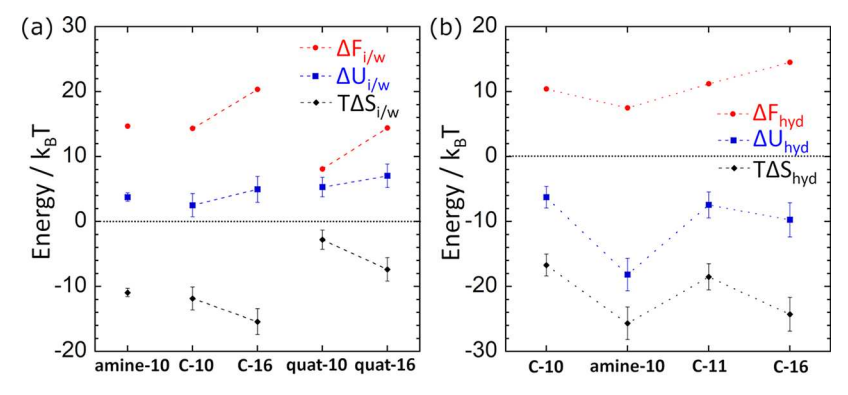


Figure 7. (a) Enthalpic—entropic contributions of the transfer free energy of the quat, amine, and alkane molecules. It is observed that $\Delta F_{i/w}^{quat}$ $^{-10}$ < $\Delta F_{i/w}^{quat}$ $^{-10}$ $\approx \Delta F_{i/w}^{amine}$ $^{-10}$ and $T\Delta S_{i/w}^{overall}$ $^{(amine-10 \ system)}$ $< T\Delta S_{i/w}^{overall}$ $^{(quat-16 \ system)}$ $< T\Delta S_{i/w}^{overall}$ $^{(quat-10 \ system)}$. (b) Enthalpic—entropic contributions of the hydration free energy of C-10, C-16, and C-11 alkanes 25 and the amine molecule. It is observed that $\Delta F_{hyd}^{amine-10}$ $< \Delta F_{hyd}^{C-10}$ $< \Delta F_{hyd}^{C-11}$ and $T\Delta S_{hyd}^{overall}$ $^{(amine-10 \ system)}$ $< T\Delta S_{hyd}^{overall}$ $^{(C-10 \ system)}$.

and their corresponding alkanes. A drop in the enthalpies of quat molecules at $\xi \approx 23$ Å accompanies the breaking of the water finger. As the free energy profiles do not show any drop at $\xi \approx 23$ Å, this implies that the disappearance of the water finger is associated with an energy-entropy compensation. It is worth noting that the extent of rise in the enthalpy profiles owing to the formation of the water finger beyond $\xi \gtrsim 12$ Å far exceeds the extent of drop in the enthalpy profiles at $\xi \approx 23$ Å. This is expected because disappearance of the water finger at ξ \approx 23 Å causes the polar headgroup to lose the solvation of the water molecules, which adds an unfavorable contribution to the enthalpy profiles. The entropy profiles, deduced from the difference between the free energy profiles and the enthalpy profiles, are shown in Figure S10 [Supporting Information]. It is interesting to note that the system entropy increases when the size of the water finger increases and drops when the water finger is broken. Both these observations align with the understanding that the entropy of the system increases (decreases) with the increase (decrease) in the air-water interfacial area. Beyond $\xi \approx 23$ Å, the quat molecules drag a few (1 to 5) water molecules with themselves in the air. We have noticed that the presence of these water molecules causes large fluctuations in the enthalpy profiles in bulk air. Figure 6b compares the enthalpy of hydration, ΔU_{hyd} and the enthalpy change of the molecules as they transfer from the interface to

the bulk aqueous phase, referred to as the interface transfer enthalpy $\Delta U_{i/w}$. The ΔU_{hyd} of the quat molecules are not accurately determined because of the large fluctuations in their enthalpy profiles beyond $\xi \gtrsim 23$ Å. The ΔU_{hyd} of the amine-10, C-10 and C-16 molecules are negative (favorable), with $\Delta U_{hyd}^{amine-10} < \Delta U_{hyd}^{C-16} < \Delta U_{hyd}^{C-10}$. We find that, for the studied molecules, $\Delta U_{i/w} > 0$. This is because as the molecules transfer from the interface to water, their alkyl tail gets submerged, which results in the loss of water—water interactions, leading to an unfavorable change in the total internal energy. $^{2.5}$

The transfer entropy, $T\Delta S_{i/w}$ is calculated using the relation,

$$T\Delta S_{i/w} = \Delta H_{i/w} - \Delta F_{i/w} \tag{3}$$

and is also shown in the Figure 7a. We find that $T\Delta S_{i/w} < 0$ for all the studied molecules. The entropy loss can be broken down into two components as

$$T\Delta S_{i/w}^{overall} = T\Delta S_{i/w}^{surfactant} + T\Delta S_{i/w}^{water}$$
(4)

where $T\Delta S_{i/w}^{surfactant}$ and $T\Delta S_{i/w}^{water}$ capture the entropic changes of the surfactant molecule and the water molecules, respectively. In the below discussion, we justify our assertion that surfactants gain entropy as they transfer from the interface to the aqueous medium. First, the translational entropy is lower at the interface because a surfactant molecule explores only a

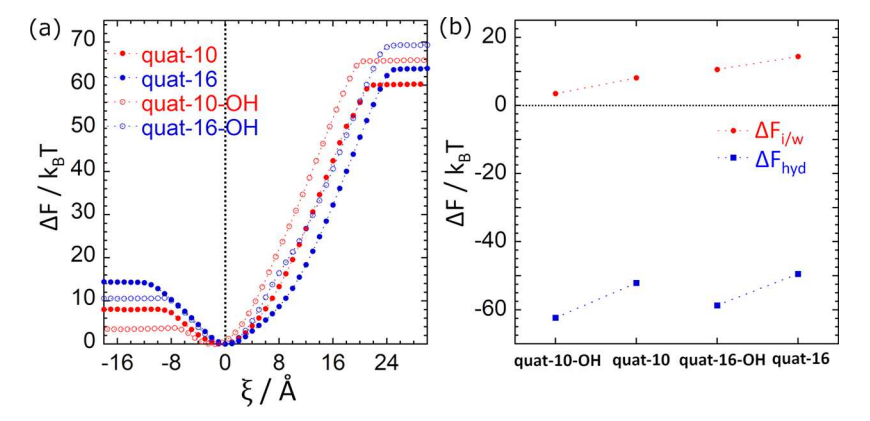


Figure 8. (a) Free energy profiles of quat-10-OH, quat-16-OH, quat-10, and quat-16 molecules with respect to distance of their center-of-mass from the air—water interface, ξ . (b) Comparison of the $\Delta F_{l/w}$ and ΔF_{hyd} values of the studied molecules in part a. The size of the error bars in the free energy values in parts a and b are within 0.3 k_BT and are therefore smaller than the size of the markers.

two-dimensional interface, whereas in the bulk aqueous phase it explores a three-dimensional region. Second, from the distributions of orientation of the surfactant molecules at the interface and in the bulk aqueous phase [Figures 5a,b and S9 (Supporting Information)], it is clear that the rotational entropy is smaller at the interface. This is because at the interface the surfactant molecules do not sample all possible orientations, unlike in the bulk aqueous phase. Last, we find that the intramolecular energy of the surfactants remains the same as the molecules transfer from bulk air to the interface and to the aqueous medium [Figure S11, Supporting Information]. The radius of gyration of the molecules does not exhibit any change. We surmise from these observations that the entropy associated with the internal degrees of freedom does not change much. Therefore, the overall entropy associated with the surfactant must increase as the surfactant transfers from the interface to the bulk aqueous phase, i.e., $T\Delta S_{i/w}^{surfactant (quat systems)} > 0$. The eq 4 therefore suggests that although $T\Delta S_{i/w}^{surfactant (quat systems)} > 0$, the loss in the entropy of water molecules causes the overall entropy of transfer of the quat molecules into water to be negative. In our prior work, we have determined that the hydration of linear alkanes results in the entropic loss of water molecules, and the entropic loss increases with the alkane length, and so, $T\Delta S_{i/w}^{water~(quat~-~16~system)}$ $< T\Delta S_{i/w}^{water (quat - 10 \text{ system})}$. This supports our observation that $T\Delta S_{i/w}^{overall (quat - 16 \text{ system})} < T\Delta S_{i/w}^{overall (quat - 10 \text{ system})}$ [Figure 7a]. We hypothesize that the loss in entropy of water near small hydrophobic solutes is attributed to the restricted conformational degrees of freedom of the water molecules.

The enthalpic—entropic breakdown of the ΔF_{hyd} of the amine molecule along with the C-10, C-16 and C-11 (obtained from our previous work²⁵) molecules are shown in Figure 7 (b). We find that $T\Delta S_{hyd}^{overall\ (amine-10\ system)} < T\Delta S_{hyd}^{overall\ (C-11\ system)}$. Since the only difference between the amine-10 and C-11 molecule is the presence of nitrogen atom in place of carbon atom, we postulate that the large entropic loss is attributed to the organization of water molecules around the polar nitrogen atom of the amine group.

3.3. Free Energy Profiles of Quaternary Ammonium –OH Molecules. The ΔF_{hyd} of quat-10 and quat-16 are found to be $-52.1~k_BT$ and $-49.5~k_BT$ respectively [Figure 4b]. Therefore, increasing the alkyl tail length decreases the solubility of these surfactants roughly by an order of magnitude. We explore if the solubility can be improved by introducing a polar moiety as the terminal group of the alkyl

tail. Previous works of Zhao et al. and Wang et al. have reported gain in the aqueous solubility upon the addition of a hydroxyl group to the headgroup. 48,49 On the other hand, Arachchi et al. have not reported any change in the aqueous solubility due to the addition of a hydroxyl group to the polar head.²⁴ One reason could be that since they added the hydroxyl group next to the oxyethylene group, which itself is a bigger polar moiety, there is little change in the overall polarity of the headgroup. Here, we have tested the effect of adding a hydroxyl group to the terminal position of the hydrocarbon tail instead of the headgroup. To this end, we replace the terminal methyl group with a hydroxyl group (-OH) in the quat-10 and quat-16 molecules. We call these as quat-10-OH and quat-16-OH [Figure 1c]. Figure 8a show the free energy profiles of quat-10-OH and quat-16-OH molecules along with the free energy profiles of the quat-10 and quat-16 molecules. From Figure 8b, an appreciable decrease of 10.2 k_BT and 9.2 k_BT in the ΔF_{hvd} is observed for the quat-10-OH and quat-16-OH with respect to the quat-10 and quat-16 molecules, respectively. Therefore, addition of a terminal -OH group is expected to significantly enhance the aqueous solubility of these surfactant molecules.

Upon their transfer from air to the interface, the free energy change of quat—OH molecules is larger in magnitude (more favorable) than their corresponding quat molecules. This observation is nontrivial because of the two counter-effects: at the interface, the —OH group tends to remain solvated (favorable), but the alkyl tail of the quat—OH molecules also gets submerged in water (unfavorable). As the quat—OH molecule moves away from the interface to the air, the —OH group loses its solvation water molecules.

Parts a and b of Figure 9 show snapshots of the configurations of quat-10-OH and quat-16-OH at the air—water interface. It is observed that the —OH group has a tendency to remain solvated and hence the alkyl tail does not protrude toward air. The spatial and orientational distributions of the quat—OH molecules are shown in Figures S12 and S13 [Supporting Information]. An appreciable decrease of $4.6~k_BT$ and $3.8~k_BT$ in the interface transfer free energies, $\Delta F_{i/w}$, is also observed for the quat-10-OH and quat-16-OH molecules with respect to the quat-10 and quat-16 molecules, respectively. A difference of $0.8~k_BT$ is observed in the reduction of $\Delta F_{i/w}$ of quat-10 ($4.6~k_BT$) and quat-16 ($3.8~k_BT$) molecules upon the introduction of an —OH group in their tails. This difference arises because of the bending of the alkyl tails of the quat—OH

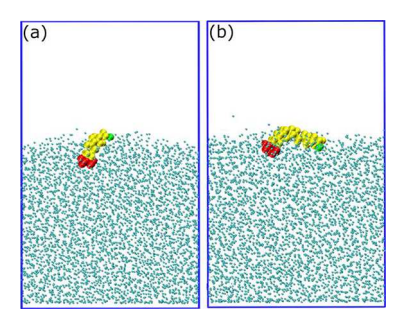


Figure 9. Simulation snapshot of (a) quat-10-OH, and (b) quat-16-OH molecules at the interface. The hydroxyl groups, as represented by the green beads, show good affinity for water and aid in bringing the hydrophobic tails toward water. Also refer to the simulation snapshot of quat-10 molecule in Figure S14a [Supporting Information] for comparison.

molecules at the interface. The snapshots of parts a and b of Figure 9 show that, at the interface, quat-16-OH has a greater number of methylene groups bent toward water than quat-10-OH. In the absence of -OH groups; however, nearly all the methylene groups of the quat molecules protrude toward air [refer to Figure S14a, Supporting Information]. Therefore, quat-16-OH experiences a little lower benefit in the reduction of the $\Delta F_{i/w}$ than quat-10-OH molecule. Enthalpy profiles of the quat-OH molecules and the enthalpic-entropic decomposition of their transfer free energies are given in Figure S15 [Supporting Information]. A smaller entropic loss in magnitude is seen upon transfer of quat-OH molecules from interface to bulk water than the quat molecules. This is likely because the alkyl tail, when the quat-OH molecules are at the interface, is already submerged in water.

3.4. Micellization Tendency of quat-OH Molecules. We have shown previously that the quat-10 and quat-16 molecules form spherical micelles above the critical micelle concentration.31,32 A micelle of 18 quat-10 molecules experiences a free energy barrier of $\sim 5 \ \hat{k_B} T$ to adsorb onto the metal—water interface. 31,32 The slow kinetics of adsorption of surfactant micelles can significantly reduce the efficacy of corrosion inhibition in oil pipelines. Therefore, it is preferable to suppress the micellization tendency of surfactants for corrosion inhibition applications. In a previous computational study, micellization free energy was computed using free energy perturbation technique and was found to be entropically driven.⁵⁰ While it is computationally challenging to calculate the micellization free energy, we have tested the tendency of quat-10-OH molecules to form micelles by starting with an initial configuration in which 18 quat-10-OH molecules are placed as a single aggregate in the bath of 4,079 water molecules [Figure 10a]. We perform MD simulation of the system in the isothermal-isobaric ensemble (fixed number of atoms N, pressure P, and temperature T) for 50 ns. It is observed that the aggregate is not stable, and the quat-10-OH molecules disintegrate in the aqueous phase [Figure 10b]. In our previous works on quat-10 and quat-16, we have observed that micelles form even when the surfactant molecules are placed randomly in the initial configuration in the aqueous medium.

We define aggregation number as the number of quat-10-OH molecules that are part of the largest aggregate in the system. In the initial configuration, the aggregation number is 18. Figure 11a shows the aggregation number of the molecules as a function of the simulation time. The initial aggregate is found

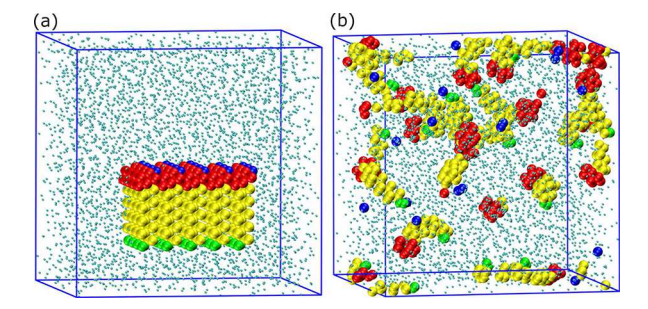


Figure 10. (a) Initial configuration of the 18 quat-10-OH molecules arranged as a single aggregate. (b) Final configuration of the quat-10-OH molecules after a MD simulation of 50 ns. The red beads represent the polar head groups, the yellow beads represent the hydrophobic alkyl tails, the green beads represent the hydroxyl groups, the blue beads represent the chloride counterions, and the small cyan dots represent the water oxygen atoms.

to disintegrate into the individual molecules within the first 10 ns of the MD simulation. The quat-10-OH molecules stay in the aggregation number of ~2 for rest of the 40 ns without showing any tendency to aggregate. Figure 11b shows the radial distribution function (RDF) between the oxygen atoms of the quat-10-OH molecules and water molecules. A large peak in the RDF at 2.6 Å indicates that there is hydrogen bonding between the hydroxyl group of the quat-10-OH molecules and water molecules. For comparison, the RDF between the nitrogen atoms of the surfactant molecules and water molecules is also plotted. The strong interaction between the hydroxyl group and water molecules supplements our understanding of why the quat-10-OH molecules do not form micelles. Reduction in the aggregation number of micelle upon substitution of a methyl group with a polar functional group is also observed experimentally by Medoš et al.⁵¹

3.5. Hydration of a Water Molecule and Hydration Free Energy Profiles of Alkanes Using the TraPPE-UA Force Field. To check the correctness of our umbrella sampling simulation procedure in determining the hydration thermodynamics, we have calculated self-hydration of a single water molecule. Figure 12a shows the free energy and enthalpy profiles of a water molecule across the air—water interface. The peak in the enthalpy profile corresponds to the formation of a water finger at $\xi = 5$ Å. In bulk air, a single water molecule exists, unlike the cationic quat molecules, which drag a few water molecules with themselves. Snapshots of the water molecule at $\xi = 5$ Å and in the bulk air ($\xi = 17.5$ Å) are shown in Figure S16 [Supporting Information].

The ΔF_{hyd} , ΔU_{hyd} , and $T\Delta S_{hyd}$ of a single water molecule are obtained as $-11.4\pm0.3~k_BT$, $-19.1\pm0.6~k_BT$, and $-7.7\pm0.7~k_BT$ respectively. We find that these estimates match well with the experimental values of $-11~k_BT$, $-17~k_BT$, and $-6~k_BT$ respectively. Our values also match well with another MD study which employed thermodynamic integration to obtain the hydration thermodynamics of a SPC/E water molecule. They report ΔF_{hyd} , ΔU_{hyd} and $T\Delta S_{hyd}$ to be $-11.8~k_BT$, $-19.65~k_BT$, and $-7.85~k_BT$ respectively.

We have also validated our results for the hydration free energy of alkanes by considering the TraPPE-UA force field of alkanes. In Figure 12b, the free energy profiles of alkanes from the TraPPE-UA force field are shown. Interestingly, the free energy profiles closely match with those from GAFF, indicating that different force fields (GAFF and TraPPE-UA) do not affect the hydration behavior of the alkanes.

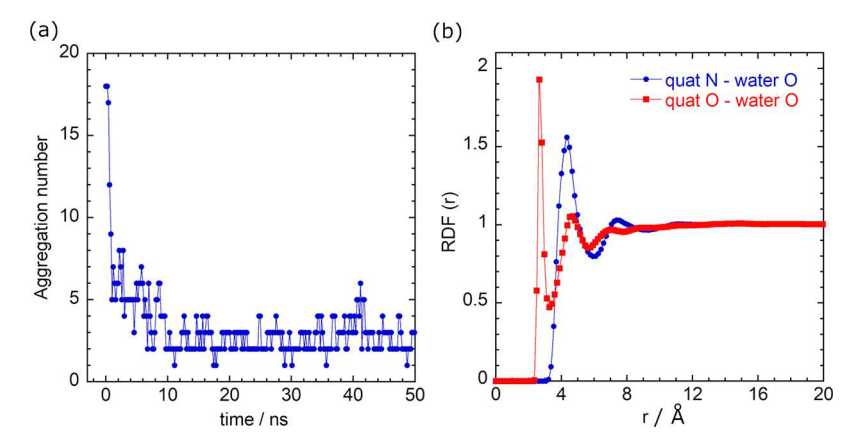


Figure 11. (a) Aggregation number of the system during the MD simulation. The aggregate is identified by utilizing the density-based spatial clustering of applications with noise (DBSCAN) algorithm. (b) RDF between the oxygen/nitrogen atoms of the quat-10-OH molecules and the oxygen atoms of the water molecules.

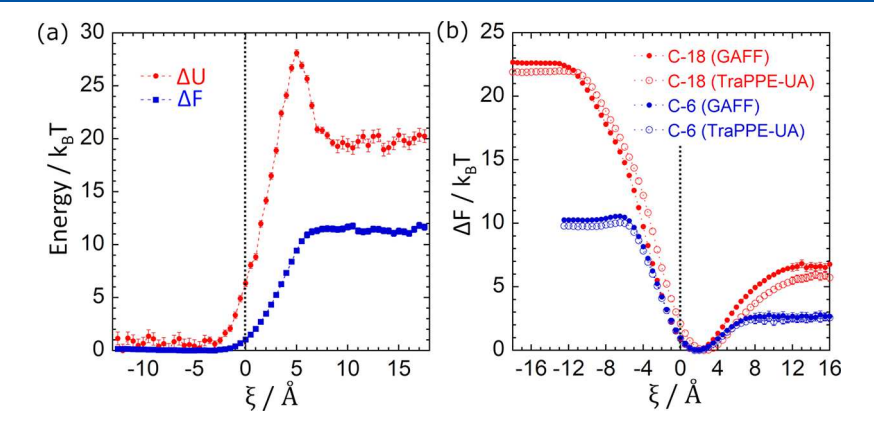


Figure 12. (a) Free energy and enthalpy profiles of a single water molecule across the air—water interface. Because of the polarity of the water molecule, a water finger is formed. The peak in the enthalpy profile at $\xi = 5$ Å correspond to the formation of water finger, as seen in case of the quat molecules. (b) Free energy profiles of C-6 and C-18 of the TraPPE-UA force field across the air—water interface. The free energy profiles obtained using TraPPE-UA force field closely match closely those obtained using GAFF.

ı

In this work, we have focused on understanding the molecular characteristics of surfactants that influence their aqueous solubility in the limit of infinite dilution. In many applications, such as corrosion inhibition, the next step involves self-assembly of surfactants at metal—water interfaces to form a well-packed layer, which amounts to a local increase in their concentration. The relevant time scales involved in the self-assembly are dictated by the diffusion of the surfactant molecules from the bulk to the metal—water interface, as well as their arrangement in ordered layers. Our previous works have focused on understanding the assembly of surfactants at the metal—water interfaces. ^{29–32,54–56}

4. CONCLUSIONS

In this work, we have studied the hydration free energy as well as the free energy of transfer from the air—water interface to the bulk aqueous phase of various surfactant molecules. We find that cationic surfactants have strongly favorable hydration free energy, while charge-neutral amine-based surfactants have marginally positive (unfavorable) hydration free energy. The contribution of the quaternary ammonium group in reducing the hydration free energy is estimated to be as large as $\sim 63~k_BT$ and that of the charge-neutral amine group to be 3 k_BT . Both surfactants and alkanes prefer to be at the air—water interface. The interface transfer free energy of these surfactants is both

enthalpically as well as entropically unfavorable. The enthalpic loss is attributed to the loss of water—water interactions. While surfactant molecules gain entropy as they transfer from the interface to the aqueous phase, water molecules experience a loss in the entropy. We find that addition of a hydroxyl group to the terminal position of the alkyl tails of the cationic quat molecules decreases the hydration free energy by 10 k_BT , which suggests a significant enhancement in their aqueous solubility. Besides improving the aqueous solubility, the hydroxyl group inhibits the formation of micelles.

ASSOCIATED CONTENT

Supporting Information

The Supporting Information is available free of charge at https://pubs.acs.org/doi/10.1021/acs.jpcb.2c03562.

Interaction potential between the bottom wall and the water molecules [eq S1]; partial charges and interaction potential parameters of the surfactant molecules [Figures S1 and S2]; water density as a function of distance from the bottom wall, z [Figure S3]; histograms of the biased distributions of quat-16 molecule (charged system) in the umbrella sampling windows [Figure S4]; snapshots of the charge-neutral system with quat-16 at (a) ξ = 24.5 Å (when moved from air-to-water), (b) ξ = 23 Å (when moved from air-to-water), (c) ξ = 24.5 Å (when moved

from water-to-air), and (d) ξ = 28 Å (when moved from water-to-air) [Figure S5]; snapshot of simulation box for (a) quat-10 molecule at $\xi = 16$ Å (air), (b) amine-10 molecule at $\xi = 16$ Å (air), and (c) C-10 molecule at $\xi =$ 16 Å (air) [Figure S6]; distributions of nitrogen of polar headgroup and carbon of terminal methyl group of (a) quat-10 and (b) quat-16 molecules when they are present at the air-water interface [Figure S7]; (a) distributions of nitrogen of polar headgroup and carbon of terminal methyl group of amine-10 molecule at the air-water interface and (b) distribution of orientation of amine-10 molecule at the interface [Figure S8]; distribution of orientation of (a) quat-10, and (b) quat-16 molecules in the bulk water [Figure S9]; entropy profiles of the quat, amine, and alkane molecules as a function of the distance of their center-of-mass from the air-water interface, ξ [Figure S10]; intramolecular energies of the quat and alkane molecules as a function of the distance of their center-of-mass from the airwater interface, ξ [Figure S11]; distributions of nitrogen of polar headgroup and oxygen of hydroxyl group of (a) quat-10-OH, and (b) quat-16-OH molecules when they are present at the air-water interface [Figure S12]; distribution of orientation of (a) quat-10-OH, and (b) quat-16-OH molecules at the interface [Figure S13]; snapshot of simulation box for (a) quat-10 molecule at ξ = -1 Å (free energy minimum location), (b) amine-10 molecule at $\xi = 2$ Å (free energy minimum location), and (c) C-10 molecule at $\xi = 2$ Å (free energy minimum location) [Figure S14]; (a) enthalpy profiles of the quat-10-OH and quat-16-OH molecules as a function of the distance of their center-of-mass from the air-water interface, ξ , and (b) enthalpic-entropic contributions of the transfer free energy of quat-OH along with the quat molecules [Figure S15]; and snapshots for hydration of a single water molecule with the water molecule (enlarged in red) at (a) $\xi = 5 \text{ Å}$, and (b) $\xi = 17.5 \text{ Å}$ [Figure S16] (PDF)

AUTHOR INFORMATION

Corresponding Author

Sumit Sharma — Department of Chemical and Biomolecular Engineering, Ohio University, Athens, Ohio 45701, United States; orcid.org/0000-0003-3138-5487; Email: sharmas@ohio.edu

Author

Himanshu Singh – Department of Chemical and Biomolecular Engineering, Ohio University, Athens, Ohio 45701, United States; ⊚ orcid.org/0000-0002-8437-686X

Complete contact information is available at: https://pubs.acs.org/10.1021/acs.jpcb.2c03562

Notes

The authors declare no competing financial interest.

ACKNOWLEDGMENTS

We thank the anonymous reviewers for their insightful comments on our first submission. This work is supported by the NSF CAREER grant 2046095. The authors thank the researchers at the Institute for Corrosion and Multiphase Technology (ICMT), Ohio University, for useful discussions.

This research used resources of the Oak Ridge Leadership Computing Facility at the Oak Ridge National Laboratory, which is supported by the Office of Science of the U.S. Department of Energy under Contract No. DE-AC05-00OR22725. Computational resources for this work were also provided by the Ohio Supercomputer Center (Project Number PAA0031), and National Science Foundation XSEDE Grant Number DMR190005.

REFERENCES

- (1) Falbe, J.Surfactants in Consumer Products: Theory, Technology and Application. Springer Science & Business Media: 2012.
- (2) Somasundaran, P.; Ramachandran, R., Surfactants in Flotation. In *Surfactants in Chemical/Process Engineering*; Routledge: 2017; pp 195–236.
- (3) Murphy, C. J.; Sau, T. K.; Gole, A. M.; Orendorff, C. J.; Gao, J.; Gou, L.; Hunyadi, S. E.; Li, T. Anisotropic Metal Nanoparticles: Synthesis, Assembly, and Optical Applications. *J. Phys. Chem. B* **2005**, 109 (29), 13857–13870.
- (4) Malik, M. A.; Hashim, M. A.; Nabi, F.; Al-Thabaiti, S. A.; Khan, Z. Anti-Corrosion Ability of Surfactants: A Review. *Int. J. Electrochem. Sci.* **2011**, 6 (6), 1927–1948.
- (5) Massarweh, O.; Abushaikha, A. S. The Use of Surfactants in Enhanced Oil Recovery: A Review of Recent Advances. *Energy Reports* **2020**, *6*, 3150–3178.
- (6) Biresaw, G., Surfactants in Lubrication. In *Lubricant Additives*; CRC Press: 2017; pp 321–336.
- (7) Panagiotopoulos, A. Z.; Floriano, M. A.; Kumar, S. K. Micellization and Phase Separation of Diblock and Triblock Model Surfactants. *Langmuir* **2002**, *18* (7), 2940–2948.
- (8) Puvvada, S.; Blankschtein, D. Molecular-Thermodynamic Approach to Predict Micellization, Phase Behavior and Phase Separation of Micellar Solutions. I. Application to Nonionic Surfactants. J. Chem. Phys. 1990, 92 (6), 3710–3724.
- (9) Ibrahim, S.Corrosion Inhibitors in the Oilfield. 2011.
- (10) Abd El-Lateef, H. M.; Abbasov, V. M.; Aliyeva, L. I.; Ismayilov, T. A. Corrosion Protection of Steel Pipelines Against CO2 Corrosion-A Review. *Chemistry J.* **2012**, *2* (2), 52–63.
- (11) Ayello, F.; Robbins, W.; Richter, S.; Nešic, S.Crude Oil Chemistry Effects on Inhibition of Corrosion and Phase Wetting. In *CORROSION 2011*; OnePetro: 2011.
- (12) Gulbrandsen, E.; Kvarekvål, J. Effect of Oil-in-Water Emulsions on the Performance of Carbon Dioxide Corrosion Inhibitors. *Corrosion* **2007**, *63* (2), 187–196.
- (13) Horsup, D.; Clark, J.; Binks, B.; Fletcher, P.; Hicks, J. The Fate of Oilfield Corrosion Inhibitors in Multiphase Systems. *Corrosion* **2010**, *66* (3), 036001–036001–14.
- (14) Knag, M. Fundamental Behavior of Model Corrosion Inhibitors. J. Disper. Sci. Technol. 2006, 27 (5), 587–597.
- (15) Horsup, D. I.; Clark, J. C.; Binks, B. P.; Fletcher, P. D.; Hicks, J. T.I Put It In, But Where Does It Go?-The Fate of Corrosion Inhibitors in Multiphase Systems. In *CORROSION 2007*; OnePetro: 2007.
- (16) McMahon, A. The Mechanism of Action of an Oleic Imidazoline Based Corrosion Inhibitor for Oilfield Use. *Colloids Surf.* **1991**, *59*, 187–208.
- (17) Knag, M.; Sjöblom, J.; Gulbrandsen, E. Partitioning of a Model Corrosion Inhibitor in Emulsions. *J. Disper. Sci. Technol.* **2006**, 27 (1), 65–75.
- (18) Zahariev, T. K.; Tadjer, A. V.; Ivanova, A. N. Transfer of Non-Ionic Surfactants Across the Water-Oil Interface: A Molecular Dynamics Study. *Colloid Surface A* **2016**, *506*, 20–31.
- (19) Liang, Y.; Zhang, S.; Wu, W.; Yang, F.; Gan, W.; Jia, H.; Chen, S.; Zhu, X.; Yuan, Q. Lyophobicity May not be the Main Driving Force for Long Chain Surfactants from the Bulk Phase to the Interface. *Phys. Chem. Chem. Phys.* **2018**, 20 (15), 10165–10172.
- (20) Cabani, S.; Gianni, P.; Mollica, V.; Lepori, L. Group Contributions to the Thermodynamic Properties of Non-Ionic

- Organic Solutes in Dilute Aqueous Solution. J. Solution Chem. 1981, 10 (8), 563-595.
- (21) Ferguson, A. L.; Debenedetti, P. G.; Panagiotopoulos, A. Z. Solubility and Molecular Conformations of n-Alkane Chains in Water. *J. Phys. Chem. B* **2009**, *113* (18), 6405–6414.
- (22) Gallicchio, E.; Kubo, M.; Levy, R. M. Enthalpy— Entropy and Cavity Decomposition of Alkane Hydration Free Energies: Numerical Results and Implications for Theories of Hydrophobic Solvation. *J. Phys. Chem. B* **2000**, *104* (26), 6271–6285.
- (23) Irisa, M.; Nagayama, K.; Hirata, F. Extended Scaled Particle Theory for Dilute Solutions of Arbitrary Shaped Solutes. An Application to Solvation Free Energies of Hydrocarbons. *Chem. Phys. Lett.* **1993**, 207 (4–6), 430–435.
- (24) Liyana-Arachchi, T. P.; Zhang, Z.; Ehrenhauser, F. S.; Avij, P.; Valsaraj, K. T.; Hung, F. R. Bubble Bursting as an Aerosol Generation Mechanism during an Oil Spill in the Deep-Sea Environment: Molecular Dynamics Simulations of Oil Alkanes and Dispersants in Atmospheric Air/Salt Water Interfaces. *Environ. Sci-Proc. Imp.* **2014**, *16* (1), 53–64.
- (25) Singh, H.; Sharma, S. Hydration of Linear Alkanes is Governed by the Small Length-Scale Hydrophobic Effect. *J. Chem. Theory Comput.* **2022**, *18* (6), 3805–3813.
- (26) Solomonov, B. N.; Sedov, I. A. Quantitative Description of the Hydrophobic Effect: The Enthalpic Contribution. *J. Phys. Chem. B* **2006**, *110* (18), 9298–9303.
- (27) Moradighadi, N.; Lewis, S.; Olivo, J. D.; Young, D.; Brown, B.; Nešić, S. Determining Critical Micelle Concentration of Organic Corrosion Inhibitors and its Effectiveness in Corrosion Mitigation. *Corrosion* **2021**, *77* (3), 266–275.
- (28) Belarbi, Z.; Dominguez Olivo, J.; Farelas, F.; Singer, M.; Young, D.; Nešić, S. Decanethiol as a Corrosion Inhibitor for Carbon Steels Exposed to Aqueous CO₂. Corrosion **2019**, 75 (10), 1246–1254.
- (29) Ko, X.; Sharma, S. Adsorption and Self-Assembly of Surfactants on Metal-Water Interfaces. *J. Phys. Chem. B* **2017**, *121* (45), 10364–10370.
- (30) Khan, M. R.; Singh, H.; Sharma, S.; Asetre Cimatu, K. L. Direct Observation of Adsorption Morphologies of Cationic Surfactants at the Gold Metal—Liquid Interface. *J. Phys. Chem. Lett.* **2020**, *11* (22), 9901—9906.
- (31) Singh, H.; Sharma, S. Disintegration of Surfactant Micelles at Metal-Water Interfaces Promotes Their Strong Adsorption. *J. Phys. Chem. B* **2020**, *124* (11), 2262–2267.
- (32) Singh, H.; Sharma, S. Determination of Equilibrium Adsorbed Morphologies of Surfactants at Metal-Water Interfaces Using a Modified Umbrella Sampling-based Methodology. *J. Chem. Theory Comput.* **2022**, *18* (4), 2513–2520.
- (33) Desimone, M.; Grundmeier, G.; Gordillo, G.; Simison, S. Amphiphilic Amido-Amine as an Effective Corrosion Inhibitor for Mild Steel Exposed to CO₂ Saturated Solution: Polarization, EIS and PM-IRRAS Studies. *Electrochim. Acta* **2011**, *56* (8), 2990–2998.
- (34) Hegazy, M.; Abdallah, M.; Awad, M.; Rezk, M. Three Novel Di-Quaternary Ammonium Salts as Corrosion Inhibitors for API X65 Steel Pipeline in Acidic Solution. Part I: Experimental Results. *Corros. Sci.* **2014**, *81*, 54–64.
- (35) Murphy, C. J.; Sau, T. K.; Gole, A. M.; Orendorff, C. J.; Gao, J.; Gou, L.; Hunyadi, S. E.; Li, T. Anisotropic Metal Nanoparticles: Synthesis, Assembly, and Optical Applications. *J. Phys. Chem. B* **2005**, *109*, 13857–13870.
- (36) Wang, J.; Wolf, R. M.; Caldwell, J. W.; Kollman, P. A.; Case, D. A. Development and Testing of a General Amber Force Field. *J. Comput. Chem.* **2004**, 25 (9), 1157–1174.
- (37) Frisch, M.; Trucks, G.; Schlegel, H.; Scuseria, G.; Robb, M.; Cheeseman, J.; Scalmani, G.; Barone, V.; Petersson, G.; Nakatsuji, H.; et al. *Gaussian 16* Revision A.03; Gaussian Inc.: Wallingford CT, 2016.
- (38) Berendsen, H.; Grigera, J.; Straatsma, T. The Missing Term in Effective Pair Potentials. *J. Phys. Chem.-US* **1987**, *91* (24), 6269–6271.
- (39) Joung, I. S.; Cheatham, T. E., III Determination of Alkali and Halide Monovalent Ion Parameters for Use in Explicitly Solvated

- Biomolecular Simulations. J. Phys. Chem. B 2008, 112 (30), 9020-9041.
- (40) Patel, A. J.; Varilly, P.; Chandler, D. Fluctuations of Water Near Extended Hydrophobic and Hydrophilic Surfaces. *J. Phys. Chem. B* **2010**, *114* (4), 1632–1637.
- (41) Rucker, G.; Yu, X.; Zhang, L. Molecular Dynamics Investigation on n-Alkane-Air/Water Interfaces. *Fuel* **2020**, *267*, 117252.
- (42) Elliott, R. W.; Watts, H. Diffusion of Some Hydrocarbons in Air: A Regularity in the Diffusion Coefficients of a Homologous Series. *Can. J. Chem.* **1972**, *50* (1), 31–34.
- (43) Liu, C.; McGivern, W. S.; Manion, J. A.; Wang, H. Theory and Experiment of Binary Diffusion Coefficient of n-Alkanes in Dilute Gases. J. Phys. Chem. A 2016, 120 (41), 8065–8074.
- (44) Plimpton, S. Fast Parallel Algorithms for Short-Range Molecular Dynamics. J. Comput. Phys. 1995, 117 (1), 1–19.
- (45) Torrie, G. M.; Valleau, J. P. Nonphysical Sampling Distributions in Monte Carlo Free-Energy Estimation: Umbrella Sampling. *J. Comput. Phys.* **1977**, 23 (2), 187–199.
- (46) Fiorin, G.; Klein, M. L.; Hénin, J. Using Collective Variables to Drive Molecular Dynamics Simulations. *Mol. Phys.* **2013**, *111* (22–23), 3345–3362.
- (47) Kumar, S.; Rosenberg, J. M.; Bouzida, D.; Swendsen, R. H.; Kollman, P. A. The Weighted Histogram Analysis Method for Free-Energy Calculations on Biomolecules. I. The Method. *J. Comput. Chem.* **1992**, *13* (8), 1011–1021.
- (48) Wang, Y.; Zhang, Y.; Liu, X.; Wang, J.; Wei, L.; Feng, Y. Effect of a Hydrophilic Head Group on Krafft Temperature, Surface Activities and Rheological Behaviors of Erucyl Amidobetaines. *J. Surfactants Deterg.* **2014**, *17* (2), 295–301.
- (49) Zhao, J.; Ďai, C.; Ding, Q.; Du, M.; Feng, H.; Wei, Z.; Chen, A.; Zhao, M. The Structure Effect on the Surface and Interfacial Properties of Zwitterionic Sulfobetaine Surfactants for Enhanced Oil Recovery. *RSC Adv.* **2015**, *5* (18), 13993–14001.
- (50) Shi, P.; Zhang, H.; Lin, L.; Song, C.; Chen, Q.; Li, Z. Molecular Dynamics Simulation of Four Typical Surfactants in Aqueous Solution. *RSC Adv.* **2019**, *9* (6), 3224–3231.
- (51) Medoš, Z.; Plechkova, N. V.; Friesen, S.; Buchner, R.; Bešter-Rogač, M. Insight into the Hydration of Cationic Surfactants: A Thermodynamic and Dielectric Study of Functionalized Quaternary Ammonium Chlorides. *Langmuir* **2019**, *35* (10), *3759*–*3772*.
- (52) Ben-Amotz, D.; Underwood, R. Unraveling Water's Entropic Mysteries: A Unified View of Nonpolar, Polar, and Ionic Hydration. *Acc. Chem. Res.* **2008**, *41* (8), 957–967.
- (53) Milne, A. W.; Jorge, M. Polarization Corrections and the Hydration Free Energy of Water. *J. Chem. Theory Comput.* **2019**, *15* (2), 1065–1078.
- (54) Sharma, S.; Ko, X.; Kurapati, Y.; Singh, H.; Nešić, S. Adsorption Behavior of Organic Corrosion Inhibitors on Metal Surfaces—Some New Insights from Molecular Simulations. *Corrosion* **2019**, *75* (1), 90–105.
- (55) Sharma, S.; Singh, H.; Ko, X. A Quantitatively Accurate Theory to Predict Adsorbed Configurations of Linear Surfactants on Polar Surfaces. *J. Phys. Chem. B* **2019**, *123* (34), 7464–7470.
- (56) Ko, X.; Sharma, S. A Quantitatively Accurate Theory to Predict Adsorbed Configurations of Asymmetric Surfactant Molecules on Polar Surfaces. *J. Phys. Chem. B* **2020**, *124* (26), 5517–5524.